Teknomekanik, Vol. 9, No. 1, pp. 42-59, February 2026
e-ISSN: 2621-8720 p-ISSN: 2621-9980

# Grid convergence analysis of an H-Darrieus wind turbine for multiple blade configurations

**Sanjaya Baroar Sakti Nasution[1*], Dian Morfi Nasution[1], Elang Pramudya Wijaya[2] and Oki Suprada Ompusunggu[1]**

[1] Department of Mechanical Engineering, Faculty of Engineering, Universitas Sumatera Utara, **Indonesia**
[2] Mechanical Engineering Study Program, IPB University, **Indonesia**

*Corresponding Author: sanjayabaroar@usu.ac.id
*Received:* 03 September 2025; *Revised:* 30 January 2026; *Accepted:* 04 February 2026

**Cite this** https://doi.org/10.24036/teknomekanik.v9i1.45272

**Abstract:** Mesh size and number significantly affected the accuracy of CFD simulations in wind turbine analysis. However, most studies focused solely on turbine performance, such as the blade torque or power coefficients. Therefore, this study adopted a broader perspective by analyzing the influence of mesh resolution on both aerodynamic performance and key fluid-dynamic parameters, including vorticity and pressure coefficients, for an H-type Darrieus vertical-axis wind turbine. Two-dimensional CFD simulations were performed using ANSYS Fluent with the k–ω SST turbulence model. Five mesh levels were evaluated across different blade configurations, and the Grid Convergence Index (GCI) was used to quantify discretization errors. The results indicate that increasing mesh resolution yields more stable torque predictions and improved resolution of near-wall flow features, with consistent grid-convergence behaviour observed across all blade configurations. GCI analysis shows that discretization errors consistently decrease as the mesh becomes finer. It also shows that a grid size of about 1.6 x $10^5$ cells is sufficient to keep errors below 5%. These findings show that including flow-field details in mesh sensitivity analysis gives a better way to check the accuracy of CFD simulations for Darrieus wind turbines.

**Keywords:** CFD; Darrius wind turbine; grid convergence index; vorticity



## 1. Introduction

Computational fluid dynamics (CFD) has recently been used by researchers and engineers in designing, analyzing, and optimization process in various fields [1], [2]. Some studies show that the utilization of CFD improves performance and reliability, reduces testing cost, product consistency, and factory productivity [3]. Additionally, CFD is effective for designing food 3D printing [4] and optimize the air quality in healthcare facilities [5]. Furthermore, the topics that CFD is mostly used for are aerodynamics and turbomachinery, where CFD gives various advantages in understanding fluid phenomena in reducing primary and secondary losses [6], [7], [8].

One of the benefits of using CFD in the field of aerodynamics and turbomachinery is to improve the performance of wind turbines [9]. CFD can be utilized to characterize fluid flow in a variety of turbine geometries and operational conditions. Compared to experimental method, which comprises high cost and is unable to perform a full-scale analysis, CFD provides more comprehensive data and visualization [10]. CFD has the ability to perform analysis on fluid-blade interaction, where the effect of blade geometry variations on aerodynamics characteristic can be determined comprehensively [11], [12], [13], to obtain an understanding of the stall phenomenon that can be used to predict the performance of straight blade vertical axis wind turbine [14], and to see the effect of blade pitch on a straight-bladed vertical axis wind turbine [15], [16]. Furthermore,

characterizing the blade shape can also be determined using CFD method, such as on how airfoil shape impacts the power output of a vertical axis turbine [17].

Though CFD has shown tremendous benefits, this numerical method, unfortunately, has its own challenges, especially in terms of the accuracy [18]. The accuracy and reliability of CFD in turbomachinery (wind turbine) is highly dependent on the computational setting [19], [20]. A wide range of studies have explored the importance of the simulation domain for CFD accuracy in wind turbine cases [21], [22]. This domain setting can lead to simulation inaccuracies in capturing dynamic stall, wake interaction, and other fluid-field parameters, especially after the fluid passes the blade [21]. Another critical factor influencing the accuracy of CFD is the choice of turbulence model, with options such as the Reynolds-Averaged Navier-Stokes (RANS) model, Large Eddies Simulation (LES), and Direct Numerical Simulation [23]. The turbulence model has a crucial impact on turbine performance and structural design [24]. A comparative study of turbulent models between URANS and SRS (Scale-Resolving Simulations) on a Vertical-Axis Wind-Turbine showed that the K-omega model produced the most accurate results, whereas the k-epsilon and SA models overpredicted [25]. In determining the most accurate turbulence model for CFD simulations of a Vertical Axis Wind Turbine, the realizable k-ε model yielded more accurate results than the transition-SST and K-omega models [26]. Moreover, the k–omega SST model has been more accurate and consistent with adopted results than other turbulence models (k-epsilon RNG, k-epsilon realizable, and SA model) [27]. Furthermore, another factor that cannot be ignored in influencing CFD accuracy is the mesh quality, both in terms of shape and size [28]. To verify a CFD simulation, the results must be independent of the mesh size or number [29].

Regarding mesh refinement, many studies have examined the relationship between mesh size and simulation results, such as, using a comparison between face and edge size to see the change in power coefficient on an H-Darrieus wind turbine [30] and the torque coefficient parameter as a dependent variable to ensure that the mesh used was properly and correctly [31]. Previous studies, particularly in the case of turbomachinery, have adopted a similar approach by selecting a single dependent parameter to evaluate the mesh independence against variations in mesh resolution [32], [33], [34]. However, this approach is limited by the subjective choice of the initial mesh size and refinement strategies, such as halving, doubling, or tripling the grid count. Some researchers then used the Grid Convergence Index (GCI), adapted from Roache's method, to verify the numerical calculations. By using this method, by extrapolation, a mesh size close to zero can be obtained, which is then used as the initial value for comparison to calculate the errors [35], [36], [37]. In the case of wind turbines, for example, the GCI method was used to determine the mesh size by comparing the mean power coefficient at 3 different mesh sizes, resulting that the minimum error obtained at GCI 21 was 0.043% [38]. In the same pattern and results, where the increasing number of meshes means the smaller the GCI error, the number of meshes with an error value below the minimum standard can be determined [39], [40]. Overall, grid convergence and mesh sensitivity analysis have been widely recognized as crucial steps to ensure the accuracy and reliability of CFD simulations for H-Darrieus wind turbines.

However, most existing studies assess grid convergence using a single turbine configuration and rely on a limited number of performance indicators, such as torque or power coefficient. The influence of variations in blade configuration on grid convergence behavior and discretization errors, particularly when combined with flow-field characteristics such as the pressure coefficient and vorticity, has not been widely studied. Therefore, this study aims to conduct a comprehensive grid-convergence analysis using the Grid Convergence Index (GCI) in CFD simulations of H-Darrieus wind turbines, employing multiple blade configurations as representative cases to verify the robustness and consistency of mesh sensitivity across different turbine geometries.

## 2. Methods

### 2.1 Design of H-Darrieus wind turbine

Three different H-Darrieus wind turbines, with 3, 4, and 5 blades, were used in this study, all with the same diameter (D) and height (H). Previous studies show that a symmetrical blade profile can enhance turbine aerodynamic performance compared with an asymmetrical profile. Therefore, in this study, a NACA 0015 is used [41], [42]. The turbine geometry was designed to generate small or micro power under 500 watts with a freestream velocity (U) of 8 m/s. Furthermore, because the number of blades varies and the chord length is constant, the turbine solidity also varies. Equation 1 is used to calculate the solidity.

$$\lambda = \frac{R\omega}{U_\infty} \tag{1}$$

The tip speed ratio (TSR) in this study is 2, as some studies mention that the optimum TSR of the H-Darrieus wind turbine is around 1.5 to 3.5 [43], [44]. TSR was then used to calculate the turbine blade's rotational speed using Equation 2.

$$\sigma = \frac{Nc}{D} \tag{2}$$

Moreover, the main geometric parameters of the turbine are listed in Table 1, and shown in Figure 1.

**Table 1.** Main geometrical parameters

| Parameter | Value |
|---|---|
| Radius, R | 0.5 m |
| Height, H | 1.56 m |
| Chord, c | 0.1 m |
| Airfoil | NACA 0015 |
| Blade Number | 3, 4, and 5 |
| θ | $120^0$, $90^0$, and $72^0$ |

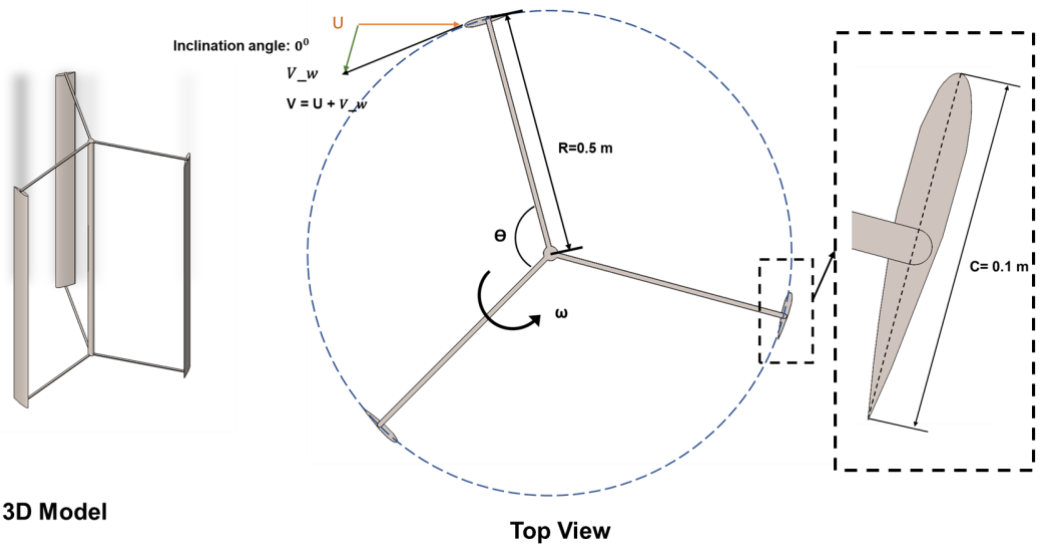


**Figure 1.** Turbine geometry

The blades are distributed along the rotor circumference with azimuthal spacings of $120^0$ for 3 blades, $90^0$ for 4 blades, and $72^0$ for 5 blades. The symmetrical NACA 0015 aerodynamic profile is used in all cases, with a constant chord length and a fixed blade inclination angle of 0°, resulting in different solidity values. The turbine geometry is represented with a two-dimensional model, Top View, with the assumption that the flow variations along the blade height is negligible. The main geometric parameters are summarized in Table 1, and the turbine geometry is illustrated in Figure 1.

## 2.2 Numerical method

Two-dimensional (2D) numerical analysis, extracted from the mid-plane of the 3D model, was done using ANSYS FLUENT licensed to the Faculty of Engineering, Universitas Sumatera Utara. It is used because 2D simulations require a smaller number of meshes compared to 3D simulations, and much literature approves that 2D simulations of Darrieus wind turbines have the ability to perform high-accuracy simulations [38]. Figure 2 displays the domain used in the simulation, which was divided into two domains, stationary rotating domain. The rotating domain is used to perform moving mesh analysis, which is the most accurate approximation for analyzing rotating equipment in CFD [45]. Moving mesh (dynamic mesh) is the unsteady numerical approach that has frequently been used, particularly in investigating the wake dynamics of the wind turbine [46]. Moving mesh (dynamic mesh) is an unsteady numerical approach that has frequently been used, particularly for investigating the wake dynamics of the wind turbine [46]. Moreover, the dimension of the geometry of the simulation depends on the diameter of the blade (D), where the flow field was expanded to achieve the fluid phenomena accuracy [12].

Figure 2 shows the boundary conditions applied, with the inlet (yellow line) as an inlet velocity of 8 m/s of a uniform wind speed. The inlet turbulence properties were defined according to the SST k–ω turbulence model. The outlet boundary (red line) was defined as a pressure outlet with a gauge pressure of 0 Pa. The backflow turbulence quantities at the outlet were set identically to those at the inlet. The upper and lower boundaries (blue lines) of the computational domain were set as symmetric boundaries, assuming that the velocity and pressure gradients perpendicular to these boundaries can be neglected. This is due to the large size of the domain relative to the rotor diameter. The rotating domain (inside the green line) containing the turbine blades is given a constant angular velocity corresponding to a rotational speed of 50 RPM. The interaction between the rotating and stationary domains is handled using a non-conformal sliding mesh interface, allowing the transient interaction between the rotor and the surrounding flow to be accurately captured. The turbine blades are arranged as nonslip walls. The SST k–ω turbulence model uses an automatic wall treatment.

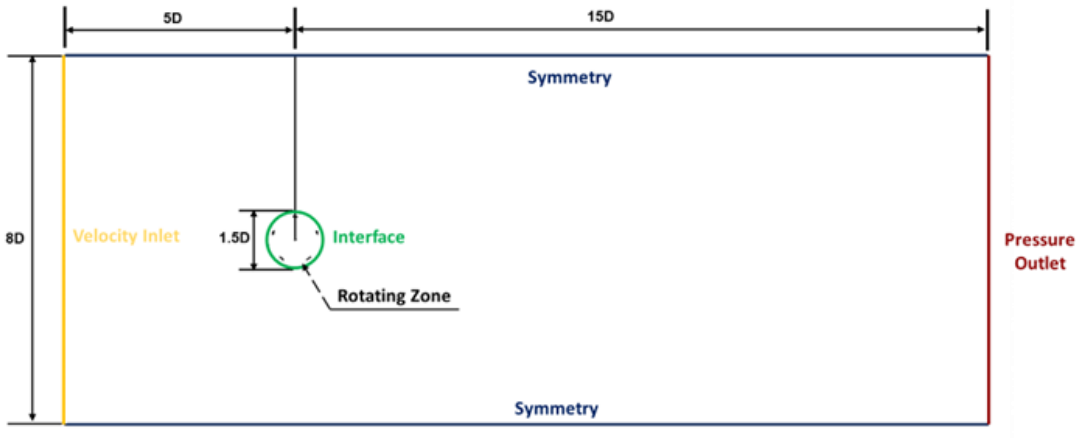


**Figure 2.** Domain and boundary conditions

The simulations were initialized using standard initialization, in which the flow field was obtained from the velocity inlet. The initial velocity, pressure, and turbulence magnitudes across the computational domain are obtained directly from the inlet boundary conditions. The rotating domain is initialized at a specified angular velocity before the transient calculation.

Simulations were performed using a pressure-based transient solver, which is well suited to unsteady flows involving a moving-mesh setup. For the discretization order, a second-order scheme was used for the pressure, momentum, and turbulence equations to improve numerical accuracy. The simulation employed a fixed time step of 0.005 s and a total of 300-time steps to adequately resolve the rotor motion and the unsteady turbulent flow. At each time step, the solution was iterated until the convergence criterion was met or the specified iteration limit was reached. Convergence was assessed based on the solver's default residual criterion for the SST k–ω turbulence model. In addition to residual-based convergence, integral quantities, such as torque and power coefficients, are also monitored.

As the flow occurred in turbulent conditions, the k-omega SST model was employed in this study. This is based on Shahizare et al., who compared 3 different RANS turbulence models in a Darrieus wind turbine (the standard k-epsilon, the standard k-omega, and the k-omega Shear Stress Transport (SST) model) and found that the k-omega SST model is the most proper model in the case of Darrieus wind turbine CFD simulation [22]. This model is a combination of standard k-omega and standard k-epsilon models, which is used to improve the model's capability to predict the flow field in the area around the wall and low Reynolds number, which is the advantage of k-omega, and flow with low adverse pressure gradient and its insensitivity in the free stream area, which is the advantage of k-epsilon [47].

Moreover, the standard 2D Navier-Stokes equations are used in this study, where Equation 3 and Equation 4 are continuity and momentum equations in differential form of Cartesian coordinates.

$$\frac{\partial(\rho)}{\partial t} + \frac{\partial(\rho u_i)}{\partial x_j} = 0 \tag{3}$$

$$\frac{\partial(\rho u_i)}{\partial t} + \frac{\partial(\rho u_i u_j)}{\partial x_j} = -\frac{\partial p}{\partial x_i} + \frac{\partial\left(\tau_{ij} - \rho u_i' u_j'\right)}{\partial x_j} + \rho g_i \tag{4}$$

Then, additional transport equations for the SST k-omega model can be seen in Equation 5 and Equation 6.

$$\frac{\partial}{\partial t}(\rho k) + \frac{\partial}{\partial x_i}(\rho k u_i) = \frac{\partial}{\partial x_j}\left(\Gamma_k \frac{\partial k}{\partial x_j}\right) + \bar{G}_k - Y_k + S_k \tag{5}$$

$$\frac{\partial}{\partial t}(\rho \omega) + \frac{\partial}{\partial x_i}(\rho \omega u_i) = \frac{\partial}{\partial x_j}\left(\Gamma_\omega \frac{\partial \omega}{\partial x_j}\right) + \bar{G}_\omega - Y_\omega + S_\omega \tag{6}$$

Compared to Standard k-ω, both the standard and SST k-ω models use the same two-equation framework. The SST variant introduces a blending function and cross-diffusion term to combine the near-wall accuracy of the k-ω model with the free-stream robustness of the k-ε model. This improves its performance in predicting separation and adverse pressure gradient flows [48].

The governing equations presented above represent the Reynolds-averaged Navier-Stokes (RANS) equations and the SST k–ω turbulence transport equations solved internally by the CFD solver.

These equations are included for theoretical completeness and reference only, and no additional user-defined implementations were implemented.

### 2.3 Grid convergence index (GCI)

Richardson extrapolation is a method used to obtain and improve the accuracy of approximations in numerical analysis and computational methods. It improves a method's results by comparing it with the same method at different levels of precision. With Richardson extrapolation, the accuracy of a numerical study is not limited to qualitative accuracy but also extends to quantitative accuracy. The basic principle of this method is to compare the results of each grid convergence test with the expected results by doubling the grid using the 2nd order method [29]. To calculate the error for each grid, the exact value of the numerical result was estimated using Equation 7.

$$f_{exact} \cong f_1 + \frac{h_2^2 f_1 - h_1^2 f_2}{h_2^2 - h_1^2} \tag{7}$$

Where h is the grid size and f is the dependent variable of the simulation, which is one parameter of the simulation's result, such as torque, pressure coefficient, etc. The comparison of h1 and h2 is defined as the grid refinement ratio, as shown in Equation 8.

$$r = \frac{h_1}{h_2} \tag{8}$$

Equation 7 then be rewritten as:

$$f_{exact} \cong f_1 + \frac{f_1 - f_2}{r^p - 1} \tag{9}$$

P is the apparent order, calculated by Equation 10.

$$P = \frac{1}{\ln (r_{21})} \left| ln \left| \frac{\varepsilon_{32}}{\varepsilon_{21}} \right| + q(p) \right| \tag{10}$$

Normally, there are at least 3 different grid sizes to be compared, where $\mathcal{E}_{32}$ and $\mathcal{E}_{21}$ are the absolute errors of these grids. Then, once the value of P is obtained, the exact solution and error can be estimated using Equation 11.

$$e_a^{21} = \left| \frac{\phi_1 - \phi_2}{\phi_1} \right| \tag{11}$$

The grid convergence index can be determined by Equation 12, where Fs is a security factor that may be defined as 1.25.

$$GCI^{21} = \frac{Fs \ e_a^{21}}{r_{21}^p - 1} \tag{12}$$

Furthermore, Figure 3 illustrates the mesh setup used in this study. The mesh inside the rotating zone is finer than in the free-stream region. This is to ensure the accuracy of the resolution of flow features around the rotating body. Along the blade surface, inflation layers were applied to the mesh to accurately capture the boundary layer phenomenon and to obtain a precise near-wall velocity gradient.

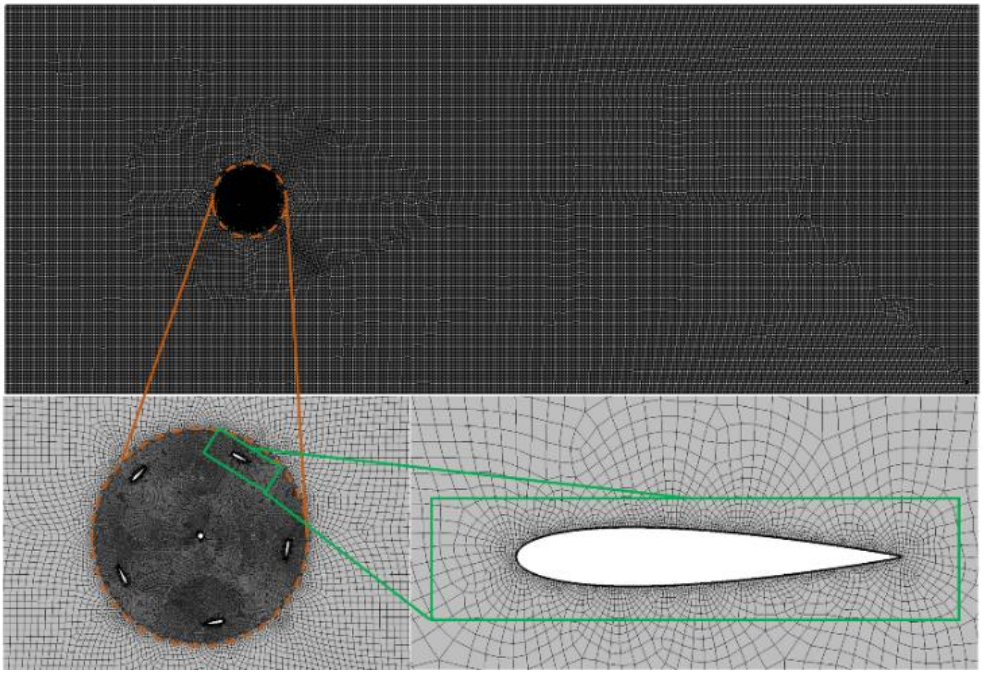

**Figure 3.** Mesh set-up

## 3. Results and discussion

### 3.1 Discretization errors

Most of the studies on grid independence techniques implement three variations of mesh refinement [49]. However, to better understand the effects of grid size and number on the performance of the Darrieus turbine, 5 grid variations were used in this study. Moreover, the study also compared grid number variation in three cases of Darrieus wind turbines. Case 1 for 3 blades, case 2 for 4 blades, and case 3 for 5 blades. The total mesh count details are in Table 2. For all blade variations, the same mesh settings are used, including inflation at the blade surface, mesh size in the rotating and stationary zones, and the names of the boundary conditions. The variation in total mesh with the number of blades is due to differences in blade size or volume. However, Table 2 shows that variations in the number of blades produce a negligible difference in the mesh count.

**Table 2.** Number of cells

| Number of blades | Grid_1 | Grid_2 | Grid_3 | Grid_4 | Grid_5 |
|---|---|---|---|---|---|
| 3 Blades | 22288 | 45311 | 89860 | 170538 | 339246 |
| 4 Blades | 21598 | 43867 | 87702 | 166571 | 333192 |
| 5 Blades | 20961 | 42703 | 85409 | 161159 | 324652 |

The performance of a Darrieus wind turbine is normally determined from the power generated by the turbine. The output power is calculated from its torque and angular velocity, where in the CFD dynamic mesh case, angular velocity is a dependent variable, and torque is an independent variable. Figure 4 shows a comparison of the effects of grid variation on the torque coefficient (Ct). Figure 4a shows the comparison on 3 blades, Figure 4b on 4 blades, and Figure 4c on 5 blades. In this study, the torque coefficient is defined as the ratio between the torque obtained from CFD results (TCFD) and the torque from potential power (T_Available).

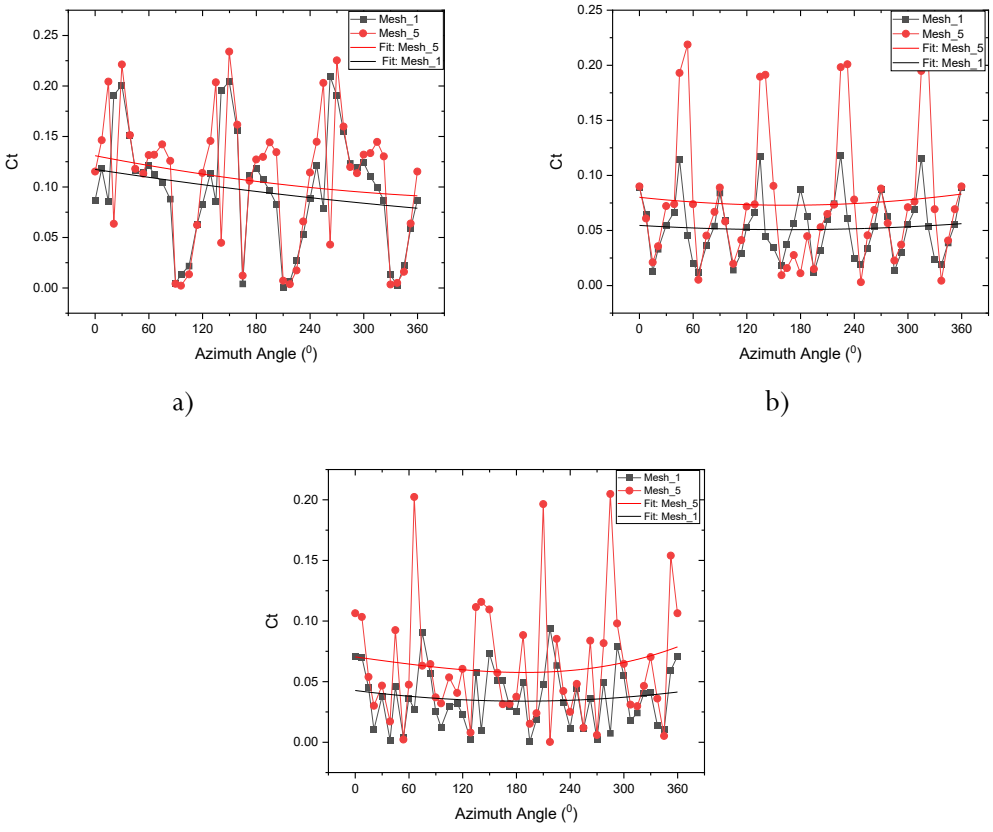


**Figure 4.** Torque Coefficient: a) 3 blades, b) 4 blades, c) 5 blades

following previous studies that also employed torque as a reference parameter for verifying their CFD simulations [50], [51]. Figure 5 shows all the torques for each value and compares the torque at each grid space. From Figure 5, it can be seen that for all runners with 3, 4, and 5 blades, higher grid spacing results in lower torque, indicating that more grids lead to lower torque. Furthermore, the graph also shows that the runner with more blades generates higher torque. However, for the runner with 5 blades, at grid space 8, the torque starts to be lower than that of the runner with 4 blades, and at grid space 16, the torque becomes closer to the torque of the runner with blade 3.

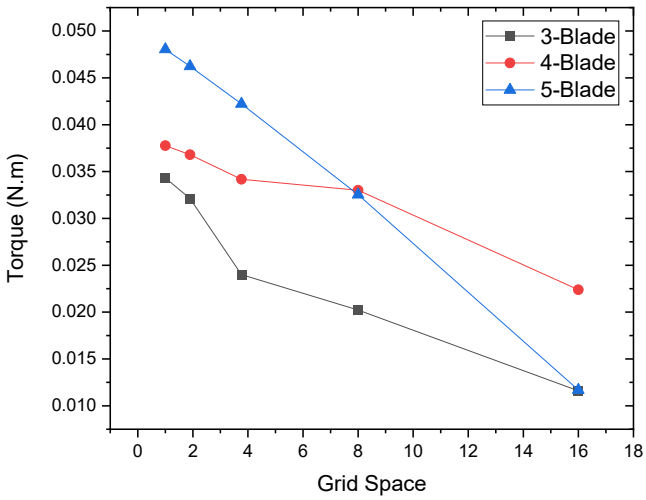


**Figure 5.** Torque of runner blades

The torque value in Figure 5 is then used to determine the GCI value. Table 3 presents the GCI calculation results for the four-blade runner. Based on Table 3, the error at GCI_12 is 1.86%, the lowest among all conditions. As for the higher error values, they are at GCI_45 with 23.39%. The results indicate that higher grid numbers lead to lower errors.

**Table 3.** GCI calculation results

| Grid normalized | Grid number | Grid spacing | Torque | GCI | |
|---|---|---|---|---|---|
| 1 | $3.2 \times 10^5$ | 1 | 0.039 | | |
| 2 | $1.6 \times 10^5$ | 1.9 | 0.038 | GC1_12 | 1.86% |
| 3 | $8.5 \times 10^4$ | 3.8 | 0.034 | GCI_23 | 5.20% |
| 4 | $4 \times 10^4$ | 8 | 0.035 | GCI_34 | 2.49% |
| 5 | $2 \times 10^4$ | 16 | 0.023 | GCI_45 | 23.39% |

Furthermore, the complete calculation results for all cases are shown in Figure 6, which presents the GCI calculations across all runner and grid number variations. The graph shows that GCI_12 achieves the lowest errors for all runners, while GCI_45 produces the highest errors. The bar chart also shows that the runner with 4 blades has the lowest error value in all cases except at GCI_45, while the runner with 5 blades has higher errors in all cases except at GCI_23. Moreover, the errors of GCI_12 for all cases are below 5%, showing that a grid number around $1.6 \times 10^5$ is acceptable. As for GCI_23, GCI_34, and GCI_45, the error rates are above 5%, excluding runners with 4 blades at GCI_34, which has an error rate of around 3%. On the contrary, GCI_45 results in more than 15% error across all blade-count variations, with the 5-blade case exceeding 60%.

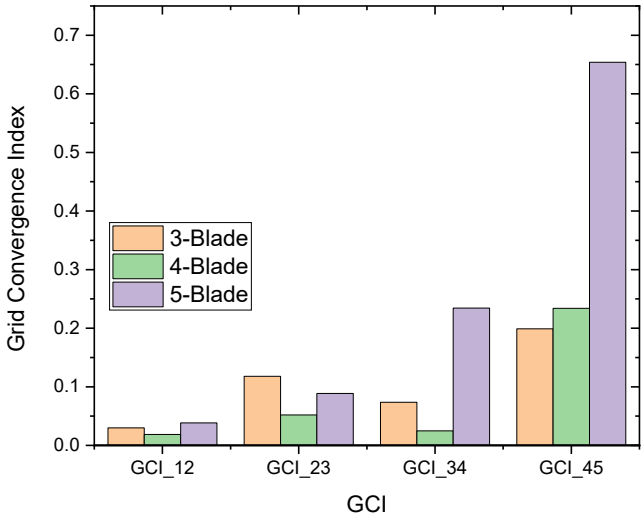


**Figure 6.** Grid convergence Index (%)

Overall, the grid convergence analysis conducted in this study serves as a numerical verification method to quantify discretization errors prior to validation. The optimal grid selection is based on the GCI threshold, solution stability, and near-wall resolution criteria; it is not compared with experimental results. However, when viewed from the stability of the resulting torque, the results of this study are consistent with previous studies using grid convergence-based verification methods or GCI, where the finer the grid size, the less fluctuating the resulting torque (see Figure 4) [19], [20], [38]. Similarly, discretization errors decreased systematically with mesh refinement, indicating that the current grid convergence behavior is in line with established numerical practice and is not a specific case [38].

### 3.2 Aerodynamics flow-field descriptions

The aerodynamic performance of Darieus wind turbine blades is governed by the characteristics of the boundary layer on the blade surface. In CFD simulations, mesh resolution in the near-wall region is essential for capturing flow phenomena such as flow separation, laminar-to-turbulent transition, and shear-stress distribution. A critical parameter in this context is the dimensionless wall distance, $Y^+$, which indicates the location of the first grid point from the wall.

#### 3.2.1 $Y^+$ on blade surface

The $Y^+$ value is important to analyze on the surface of a Darrieus wind turbine blade because it is directly related to the accuracy of boundary-layer flow predictions, which greatly affects the blade's aerodynamic performance [52]. $Y^+$ is a non-dimensional parameter that indicates how far the center point of the first grid element (mesh) is from the solid surface in viscous units. In CFD simulations, this value is important to capture viscous phenomena [53]. The boundary layer affects the lift and drag forces on the blade. If the turbulence model or mesh does not capture the near-wall zone correctly due to an inappropriate $Y^+$, then the predicted aerodynamic performance will be significantly different from the experiment [53]. Figure 7 shows the distribution of $Y^+$ values along the blade surface on three different blades (Blade 3, Blade 4, and Blade 5). This data was collected at five mesh resolutions to evaluate the quality of boundary-layer resolution on each blade. The $Y^+$ values shown in Figure 7 are the average value for all variations shown in the bar chart and the maximum and minimum $Y^+$ values on Blade 3.

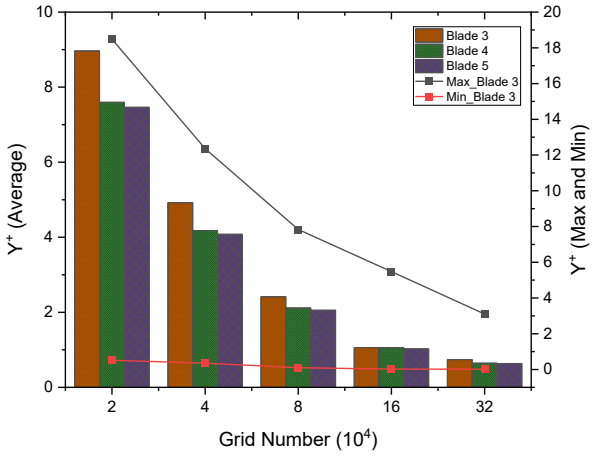


**Figure 7.** Y+ on blade surface

In general, the $Y^+$ values show a decreasing trend from the lowest to the highest mesh number. Blade 3 consistently shows the highest $Y^+$ value among the blades, indicating that the mesh around its surface is coarser or experiences more complex flow conditions. In Figure 7, lines also show the maximum and minimum $Y^+$ values on Blade 3. The minimum value remains relatively constant below 1 across the mesh number range, while the maximum value decreases significantly, similar to the average $Y^+$ value. This indicates that the mesh size on the blade surface affects the aerodynamic flow around the blade. Numerous studies imply that in simulation with K-Omega SST, the $Y^+$ value should be no more than 15 [54], [55]. Moreover, in this study, a grid number above 40000 yields an average Y+ value below 15, indicating that all mesh variations used in this study are acceptable for performing the K-Omega SST simulation, except grid_1. However, some

other studies suggest that the Y+ value should be around 1 or below, which denotes grid_4 and grid_5 as satisfactory to be implemented with the K-Omega SST model [56].

### 3.2.2 Pressure coefficient (Cp)

To understand the characteristics of airflow and pressure distribution during the conversion of wind energy into mechanical energy, analyzing the pressure distribution and its coefficient of performance (Cp) on the blade surface is crucial. Cp describes the pressure difference between the blade surface and the free stream pressure, which directly affects the lift and drag forces acting on the blade. Knowing the distribution of Cp along the blade surface enables the evaluation of the aerodynamic efficiency of the blade design and the potential for flow phenomena such as separation or turbulence. Therefore, a thorough understanding of Cp distribution is crucial for optimizing a wind turbine's overall performance.

In CFD simulations, the accuracy of Cp predictions depends on the quality and size of the mesh used. The mesh that is too coarse can lose important flow details, particularly around the boundary layer and in areas with high pressure gradients, leading to less accurate Cp predictions. In contrast, finer meshes enable more complex and accurate capture of flow phenomena, but they incur higher computational costs. Therefore, selecting the right mesh size is crucial in obtaining a representative Cp distribution on the surface of a wind turbine blade. However, Cp is determined by the equation 13.

$$C_P = \frac{P - P_\infty}{1/2\,\rho V^2} \tag{13}$$

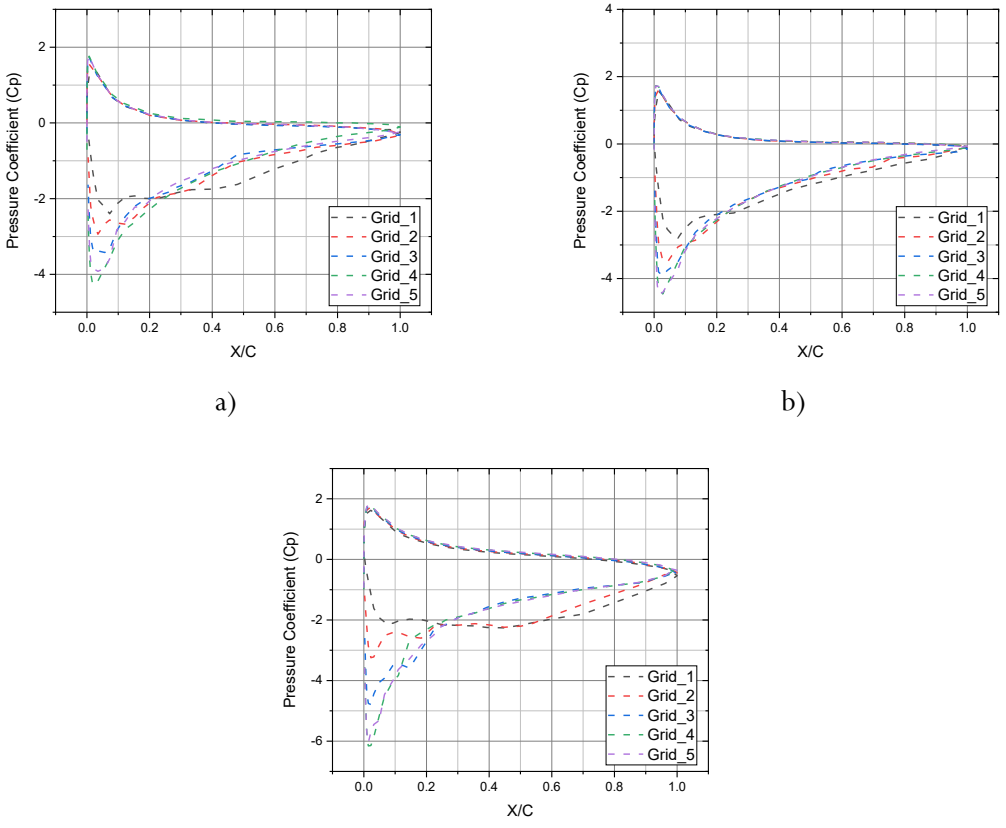


**Figure 8**. Pressure Coefficient on blade surface, a) 3 Blades, b) 4 Blades, c) 5 Blades

Figure 8 illustrates the distribution of the pressure coefficient (Cp) along the chordwise direction (X/C) of the wind turbine blade surface for five different grid resolutions, Grid_1 to Grid_5. The Cp values were obtained from numerical simulations using varying mesh numbers to evaluate the influence of grid resolution on solution accuracy. As observed, Grid_1, which represents the coarsest mesh, shows noticeable deviations in Cp, particularly near the leading edge (X/C ≈ 0.0–0.2), where the pressure gradient becomes steep, and flow separation occurs. Conversely, finer meshes (Grid_2 to Grid_5) show increasingly consistent Cp distributions, indicating improved boundary-layer resolution and more accurate pressure-field capture. The Cp distribution from Grid_3 to Grid_5 shows that grid independence is achieved at Grid_3 and beyond, with further mesh refinement yielding negligible changes in the pressure distribution. This highlights the importance of mesh refinement, particularly near regions with high curvature or sharp gradients, to ensure numerical stability and reliable aerodynamic predictions. Similar phenomena are observed in Figures 8b and 8c for blade numbers 4 and 5. Overall, Figures 8a, 8b, and 8c show that mesh size and quality are crucial for resolving the pressure distribution on the surface of blades, which affects the prediction of aerodynamic forces acting on it. These results also agree with findings from previously published numerical and experimental studies on vertical-axis wind turbines, which underscore the importance of appropriate near-wall grid resolution to accurately capture pressure gradients [25], [55].

### 3.2.3 Vorticity

The analysis of vorticity contours around the wind turbine blade provides important information about the flow field, particularly for identifying regions of flow separation, vortex formation, and boundary-layer interactions. The vorticity distribution shows how rapidly the fluid rotates near the blade surface. This directly affects the pressure distribution, aerodynamic forces, and overall turbine performance. Figure 8 shows the vortex contour around the blade. This study's vorticity analysis was performed on a single turbine blade at a fixed azimuth angle to examine the effect of grid count on the vortex phenomenon.

Figure 9 shows that the grid number affects the vortex around the blade. The vorticity contour visualization reveals a strong dependence of vortex formation on both mesh resolution and blade number. For the coarsest mesh (Mesh 1), vortex structures are barely captured, with minimal indications of flow separation near the trailing edge. As mesh resolution improves (Meshes 3 to 5), vortical structures become increasingly visible, particularly in configurations with four and five blades. In these finer meshes, periodic vortex patterns begin to emerge downstream of the airfoil, indicating the onset of vortex shedding. At the leading edge, vorticity is consistently observed across all mesh levels, though its intensity and spatial resolution improve with mesh refinement. This vorticity is primarily associated with flow acceleration and the formation of thin boundary layers. In higher-blade-number configurations, the interaction between the incoming flow and adjacent blades appears to slightly intensify the leading-edge vorticity. Overall, Figure 9 shows that the simulation with a finer mesh captures the vortex structures more accurately and reliably. This is in line with flow field characteristics reported in a previous study about Darrieus-type wind turbines [21], [30]. The studies reported that a coarser mesh is generally less capable of capturing the vortex formation and wake interactions.

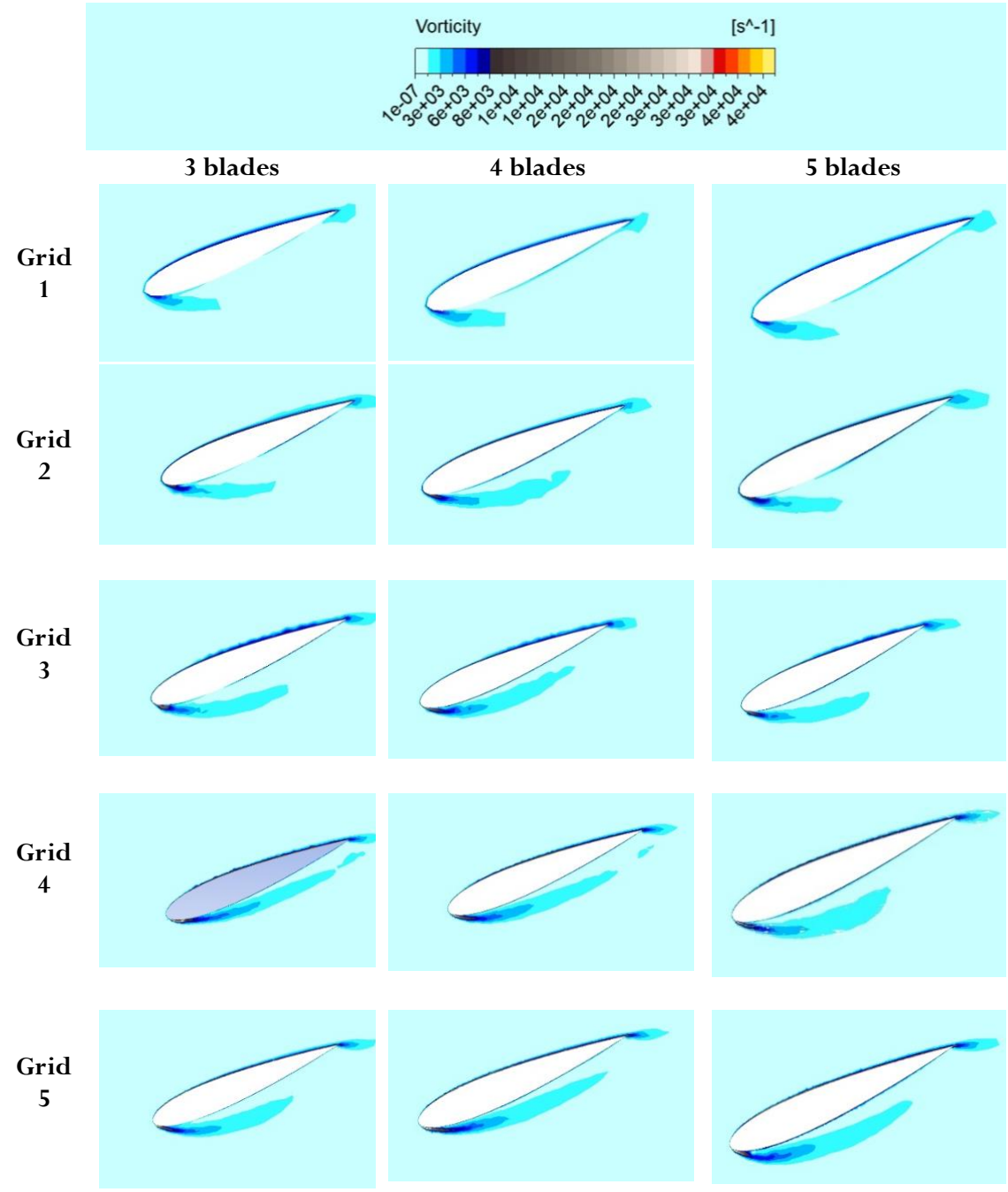


**Figure 9.** Vorticity contour

## 4. Conclusion

This study analyzes the grid convergence index for an H-type Darrieus vertical-axis wind turbine with multiple blade configurations using CFD simulations. Both turbine performance and flow characteristics are considered. The study results show that finer mesh resolutions improve turbine performance predictions and enhance the accuracy of flow-field characteristics, including boundary-layer behavior and vortex formation. GCI analysis confirmed that the error rate decreased consistently as the mesh number was increased. It is also shown that a cell count of approximately 1.6 x 105 yielded a calculated error within an acceptable margin of less than 5%. With mesh refinement, Cp distributions along the blade surface become more consistent and better capture vortex structures, especially at trailing edges and in wake regions. The results of this study highlight the importance of Grid Convergence Index assessments to ensure the reliability of CFD simulations of H vertical-axis wind turbines.

## Author's declaration

### Author contribution

**Sanjaya Baroar Sakti Nasution** initiated the project and conducted the simulation; **Dian Morfi Nasution** reviewed the numerical method and verified the results; **Elang Pramudya Wijaya** developed the mathematical modeling of GCI and examined the errors. **Oki Suprada Ompusunggu** created graphs and tables and ensured the clarity. The manuscript was written through the contribution of all authors. All authors discussed the results, reviewed, and approved the final version of the manuscript.

### Funding statement

This research was funded by the Faculty of Engineering, Universitas Sumatera Utara (FT USU), through an internal research grant under contract number: 2/UN5.2.1.4/PPM/2025.

### Data Availability

The datasets generated and/or analyzed during the current study are available from the corresponding author on reasonable request.

### Acknowledgements

The authors would like to express their sincere gratitude to the Computational Laboratory of Mechanical Engineering, Universitas Sumatera Utara (USU), for providing the computational resources and simulation facilities used in this study.

### Competing interest

The authors declared no potential conflicts of interest concerning the research, authorship, and publication of this article.

### Ethical clearance

This research does not involve humans as subjects.

### AI statement

This article is the original work of the author without using AI tools for writing sentences and/or creating/editing tables and figures in this manuscript.

## Publisher's and Journal's note

Universitas Negeri Padang as the publisher, and Editor of Teknomekanik state that there is no conflict of interest towards this article publication.

## References

[1] F. Z. Wang, I. L. Animasaun, T. Muhammad, and S. S. Okoya, "Recent Advancements in Fluid Dynamics: Drag Reduction, Lift Generation, Computational Fluid Dynamics, Turbulence Modelling, and Multiphase Flow," *Arabian Journal for Science and Engineering*, vol. 49, no. 8, pp. 10237–10249, 2024, https://doi.org/10.1007/s13369-024-08945-3

[2] M. Muktiarni, N. I. Rahayu, A. Nurhayati, A. D. Bachari, and A. Ismail, "Concept of Computational Fluid Dynamics Design and Analysis Tool for Food Industry: A Bibliometric," *CFD Letters*, vol. 16, no. 2, pp. 1–23, 2024, https://doi.org/10.37934/cfdl.16.2.123

[3] A. W. Date, "Introduction to computational fluid dynamics," *Introduction to Computational Fluid Dynamics*, vol. 9780521853, no. 2, pp. 1–377, 2005, https://doi.org/10.1017/CBO9780511808975

[4] T. M. Oyinloye and W. B. Yoon, "Application of computational fluid dynamics (Cfd) simulation for the effective design of food 3d printing (a review)," *Processes*, vol. 9, no. 11, 2021, https://doi.org/10.3390/pr9111867

[5] Hong Yee Kek *et al.*, "A CFD assessment on ventilation strategies in mitigating healthcare-associated infection in single patient ward," *Progress in Energy and Environment*, vol. 24, no. 1, pp. 35–45, 2023, https://doi.org/10.37934/progee.24.1.3545

[6] M. Giovannini, F. Rubechini, M. Marconcini, A. Arnone, and F. Bertini, "Reducing secondary flow losses in low-pressure turbines: The 'snaked' blade," *International Journal of Turbomachinery, Propulsion and Power*, vol. 4, no. 3, 2019, https://doi.org/10.3390/ijtpp4030028

[7] J. Coull, C. Clark, and R. Vazquez, "The sensitivity of turbine cascade endwall loss to inlet boundary layer thickness," *Journal of the Global Power and Propulsion Society*, vol. 3, pp. 540–554, 2019, https://doi.org/10.22261/JGPPS.OEYMDE

[8] A. Zaryankin, A. Rogalev, V. Kindra, V. Khudyakova, and N. Bychkov, "Reduction methods of secondary flow losses in stator blades: Numerical and experimantal study," *European Conference on Turbomachinery Fluid Dynamics and Thermodynamics, ETC*, no. January, 2017, https://doi.org/10.29008/etc2017-158

[9] W. Zhang, J. Calderon-Sanchez, D. Duque, and A. Souto-Iglesias, "Computational Fluid Dynamics (CFD) applications in Floating Offshore Wind Turbine (FOWT) dynamics: A review," *Applied Ocean Research*, vol. 150, no. May, p. 104075, 2024, https://doi.org/10.1016/j.apor.2024.104075

[10] Y. Li, S. Yang, F. Feng, and K. Tagawa, "A review on numerical simulation based on CFD technology of aerodynamic characteristics of straight-bladed vertical axis wind turbines," *Energy Reports*, vol. 9, pp. 4360–4379, 2023, https://doi.org/10.1016/j.egyr.2023.03.082

[11] M. A. Singh, A. Biswas, and R. D. Misra, "Investigation of self-starting and high rotor solidity on the performance of a three S1210 blade H-type Darrieus rotor," *Renewable Energy*, vol. 76, pp. 381–387, 2015, https://doi.org/10.1016/j.renene.2014.11.027

[12] D. Han, Y. G. Heo, N. J. Choi, S. H. Nam, K. H. Choi, and K. C. Kim, "Design, fabrication, and performance test of a 100-W helical-blade vertical-axis wind turbine at low tip-speed ratio," *Energies*, vol. 11, no. 6, pp. 1–17, 2018, https://doi.org/10.3390/en11061517

[13] Q. Cheng, X. Liu, H. S. Ji, K. C. Kim, and B. Yang, "Aerodynamic analysis of a helical Vertical axis wind turbine," *Energies*, vol. 10, no. 4, 2017, https://doi.org/10.3390/en10040575

[14] L. X. Zhang, Y. B. Liang, X. H. Liu, Q. F. Jiao, and J. Guo, "Aerodynamic performance prediction of straight-bladed vertical axis wind turbine based on CFD," *Advances in Mechanical Engineering*, vol. 2013, 2013, https://doi.org/10.1155/2013/905379

[15] J. Guo, T. Qu, and L. Lei, "Effect of pitch parameters on aerodynamic forces of a straight-bladed vertical axis wind turbine with inclined pitch axes," *Applied Sciences (Switzerland)*, vol. 11, no. 3, pp. 1–12, 2021, https://doi.org/10.3390/app11031033

[16] Z. Zhao *et al.*, "Variable pitch approach for performance improving of straight-bladed VAWT at rated tip speed ratio," *Applied Sciences (Switzerland)*, vol. 8, no. 6, 2018, https://doi.org/10.3390/app8060957

[17] M. R. Tirandaz and A. Rezaeiha, "Effect of airfoil shape on power performance of vertical axis wind turbines in dynamic stall: Symmetric Airfoils," *Renewable Energy*, vol. 173, pp. 422–441, 2021, https://doi.org/10.1016/j.renene.2021.03.142

[18] Y. Jiang, A. Murray, L. di Mare, and P. Ireland, "Mesh sensitivity of RANS simulations on film cooling flow," *International Journal of Heat and Mass Transfer*, vol. 182, p. 121825, 2022, https://doi.org/10.1016/j.ijheatmasstransfer.2021.121825

[19] A. Rezaeiha, H. Montazeri, and B. Blocken, "Towards accurate CFD simulations of vertical axis wind turbines at different tip speed ratios and solidities: Guidelines for azimuthal increment, domain size and convergence," *Energy Conversion and Management*, vol. 156, no. October 2017, pp. 301–316, 2018, https://doi.org/10.1016/j.enconman.2017.11.026

[20] A. Rezaeiha, I. Kalkman, and B. Blocken, "CFD simulation of a vertical axis wind turbine operating at a moderate tip speed ratio: Guidelines for minimum domain size and azimuthal increment," *Renewable Energy*, vol. 107, pp. 373–385, 2017, https://doi.org/10.1016/j.renene.2017.02.006

[21] F. Balduzzi, A. Bianchini, R. Maleci, G. Ferrara, and L. Ferrari, "Critical issues in the CFD simulation of Darrieus wind turbines," *Renewable Energy*, vol. 85, pp. 419–435, 2016, https://doi.org/10.1016/j.renene.2015.06.048

[22] B. Shahizare, N. N. Bin Nik Ghazali, W. T. Chong, S. S. Tabatabaeikia, and N. Izadyar, "Investigation of the optimal omni-direction-guide-vane design for vertical axiswind turbines based on unsteady flow CFD simulation," *Energies*, vol. 9, no. 3, 2016, https://doi.org/10.3390/en9030146

[23] D. C. Wilcox, *Turbulence Modelling for CFD 3rd Edition*. 1993.

[24] J. H. Liu, J. C. Chen, and N. T. Corbita, "Analysis and comparison of turbulence models on wind turbine performance using SCADA data and machine learning technique," *Cogent Engineering*, vol. 10, no. 1, 2023, https://doi.org/10.1080/23311916.2023.2167345

[25] A. Meana-Fernández, J. M. Fernández Oro, K. M. Argüelles Díaz, and S. Velarde-Suárez, "Turbulence-model comparison for aerodynamic-performance prediction of a typical vertical-axis wind-turbine airfoil," *Energies*, vol. 12, no. 3, pp. 1–16, 2019, https://doi.org/10.3390/en12030488

[26] M. R. Rashed, O. E. Abdellatif, M. F. Abd Rabbo, E. E. Khalil, and I. Shahin, "Turbulence Modeling Comparative Analysis for Vertical Axis Wind Turbines," *Engineering Research Journal - Faculty of Engineering (Shoubra)*, vol. 44, no. 1, pp. 71–79, 2020, https://doi.org/10.21608/erjsh.2020.290027

[27] P. I. Muiruri, O. S. Motsamai, and R. Ndeda, "A comparative study of RANS-based turbulence models for an upscale wind turbine blade," *SN Applied Sciences*, vol. 1, no. 3, pp. 1–15, 2019, https://doi.org/10.1007/s42452-019-0254-5

[28] H. Li, L. Rong, and G. Zhang, "Reliability of turbulence models and mesh types for CFD simulations of a mechanically ventilated pig house containing animals," *Biosystems Engineering*, vol. 161, pp. 37–52, 2017, https://doi.org/10.1016/j.biosystemseng.2017.06.012

[29] P. J. Roache and P. J. Roache, *Fundamentals of verification and validation*. 2009.

[30] J. G. Acosta-López, A. P. Blasetti, S. Lopez-Zamora, and H. de Lasa, "CFD Modeling of an H-Type Darrieus VAWT under High Winds: The Vorticity Index and the Imminent Vortex Separation Condition," *Processes*, vol. 11, no. 2, 2023, https://doi.org/10.3390/pr11020644

[31] P. M. Kumar, M. R. Surya, K. Sivalingam, T. C. Lim, S. Ramakrishna, and H. Wei, "Computational optimization of adaptive hybrid Darrieus turbine: Part 1," *Fluids*, vol. 4, no. 2, 2019, https://doi.org/10.3390/fluids4020090

[32] S. M. E. Saryazdi and M. Boroushaki, "2D numerical simulation and sensitive analysis of H-darrieus wind turbine," *International Journal of Renewable Energy Development*, vol. 7, no. 1, pp. 23–34, 2018, https://doi.org/10.14710/ijred.7.1.23-24

[33] P. Zamre and T. Lutz, "Computational-fluid-dynamics analysis of a Darrieus vertical-axis wind turbine installation on the rooftop of buildings under turbulent-inflow conditions,"

*Wind Energy Science*, vol. 7, no. 4, pp. 1661–1677, 2022, https://doi.org/10.5194/wes-7-1661-2022

[34] P. Queutey, G. Deng, J. Wackers, E. Guilmineau, A. Leroyer, and M. Visonneau, "Sliding grids and adaptive grid refinement for RANS simulation of ship-propeller interaction," *Ship Technology Research*, vol. 59, no. 2, pp. 44–57, 2012, https://doi.org/10.1179/str.2012.59.2.004

[35] P. J. Roache, "Roache_1994.pdf," *Journal of Fluid Engineering*, vol. 116. pp. 405–413, 1994.

[36] D. P. Sari *et al.*, "Performance of undershot waterwheel in pico scale with difference in the blades number," *Journal of the Brazilian Society of Mechanical Sciences and Engineering*, vol. 44, no. 3, pp. 1–10, 2022, https://doi.org/10.1007/s40430-022-03430-0

[37] D. Adanta, S. B. S. Nasution, Budiarso, Warjito, A. I. Siswantara, and H. Trahasdani, "Open flume turbine simulation method using six-degrees of freedom feature," *AIP Conference Proceedings*, vol. 2227, no. May, 2020, https://doi.org/10.1063/5.0004389

[38] A. Meana-Fernández, J. M. Fernández Oro, K. M. Argüelles Díaz, M. Galdo-Vega, and S. Velarde-Suárez, "Application of Richardson extrapolation method to the CFD simulation of vertical-axis wind turbines and analysis of the flow field," *Engineering Applications of Computational Fluid Mechanics*, vol. 13, no. 1, pp. 359–376, 2019, https://doi.org/10.1080/19942060.2019.1596160

[39] S. Shubham, U. Kingdom, and N. Wright, "VAWT aerodynamics and aeroacoustics at various tip speed ratios using Lattice Boltzmann Method," Authorea. pp. 1–20, 2023. https://doi.org/10.22541/au.174315443.31960751/v1

[40] G. Baca, G. B. Dos Santos, and L. O. Salviano, "Design and Optimization of a Low TSR HDarrieus Turbine Based on Geometry Parameterization Through Joukowsky Transformation," *Advances in Transdisciplinary Engineering*, vol. 54, pp. 447–459, 2024, https://doi.org/10.3233/ATDE240345

[41] Z. Zhao, D. Wang, T. Wang, W. Shen, H. Liu, and M. Chen, "A review: Approaches for aerodynamic performance improvement of lift-type vertical axis wind turbine," *Sustainable Energy Technologies and Assessments*, vol. 49, no. October 2021, p. 101789, 2022, https://doi.org/10.1016/j.seta.2021.101789

[42] A. Bianchini, G. Ferrara, and L. Ferrari, "Design guidelines for H-Darrieus wind turbines: Optimization of the annual energy yield," *Energy Conversion and Management*, vol. 89, pp. 690–707, 2015, https://doi.org/10.1016/j.enconman.2014.10.038

[43] S. Ali and C. M. Jang, "Effects of tip speed ratios on the blade forces of a small h-darrieus wind turbine," *Energies*, vol. 14, no. 13, pp. 1–18, 2021, https://doi.org/10.3390/en14134025

[44] E. Leelakrishnan, M. Sunil Kumar, D. Selvaraj, N. Sundara Vignesh, and T. S. Abhesheka Raja, "Numerical evaluation of optimum tip speed ratio for darrieus type vertical axis wind turbine," *Materials Today: Proceedings*, vol. 33, Part 7, pp. 4719–4722, 2020, https://doi.org/10.1016/j.matpr.2020.08.352

[45] C. Lothodé, J. Poncin, D. Lemosse, E. Pagnacco, and E. S. Cursi, "Efficient dynamic fluid-structure computation for blade-mast interaction of a tidal turbine," *7th International Conference on Ocean Energy 2018*, no. June, pp. 1–7, 2018. http://ocean-energy-systems.org/publications/icoe/icoe-2018/document/efficient-dynamic-fluid-structure-computation-for-blade-mast-interaction-of-a-tidal-turbine/

[46] A. Khedr and F. Castellani, "Critical issues in the moving reference frame CFD simulation of small horizontal axis wind turbines," *Energy Conversion and Management: X*, vol. 22, no. February, p. 100551, 2024, https://doi.org/10.1016/j.ecmx.2024.100551

[47] F. R. Menter, "Improved two-equation k-omega turbulence models for aerodynamic flows," 1992. https://ntrs.nasa.gov/citations/19930013620

[48] F. R. Menter, "Review of the shear-stress transport turbulence model experience from an industrial perspective," *International journal of computational fluid dynamics*, vol. 23, no. 4, pp. 305–316, 2009. https://doi.org/10.1080/10618560902773387

[49] A. Seeni, P. Rajendran, and H. Mamat, "A CFD mesh independent solution technique for low reynolds number propeller," *CFD Letters*, vol. 11, no. 10, pp. 15–30, 2019. https://www.akademiabaru.com/submit/index.php/cfdl/article/view/3187

[50] Warjito, Budiarso, K. Celine, and S. B. Sakti Nasution, "Computational Method for Designing a Nozzle Shape to Improve the Performance of Pico-Hydro Crossflow Turbines," *International Journal of Technology*, vol. 12, no. 1, pp. 139–148, 2021, https://doi.org/10.14716/ijtech.v12i1.4225

[51] M. N. Uddin, M. Atkinson, and F. Opoku, "CFD Investigation of a Hybrid Wells Turbine with Passive Flow Control," *Energies*, vol. 16, no. 9, 2023, https://doi.org/10.3390/en16093851

[52] K. Song, H. Huan, L. Wei, and C. Liu, "Aerodynamic Performance and Coupling Gain Effect of Archimedes Spiral Wind Turbine Array," *Journal of Marine Science and Engineering*, vol. 12, no. 7, 2024, https://doi.org/10.3390/jmse12071062

[53] P. K. Talukdar, A. Sardar, V. Kulkarni, and U. K. Saha, "Parametric analysis of model Savonius hydrokinetic turbines through experimental and computational investigations," *Energy Conversion and Management*, vol. 158, no. December 2017, pp. 36–49, 2018, https://doi.org/10.1016/j.enconman.2017.12.011

[54] S. V Ramana Murthy and S. Kishore Kumar, "Effect of different turbulence models on the numerical analysis of axial flow turbine stage of a typical turbofan engine," in *Gas Turbine India Conference*, American Society of Mechanical Engineers, 2013, p. V001T02A004. https://doi.org/10.1115/GTINDIA2013-3555

[55] M. Moshfeghi, Y. J. Song, and Y. H. Xie, "Effects of near-wall grid spacing on SST-K-ω model using NREL Phase VI horizontal axis wind turbine," *Journal of Wind Engineering and Industrial Aerodynamics*, vol. 107, pp. 94–105, 2012. https://doi.org/10.1016/j.jweia.2012.03.032

[56] S. Younoussi and A. Ettaouil, "Calibration method of the k-ω SST turbulence model for wind turbine performance prediction near stall condition," *Heliyon*, vol. 10, no. 1, p. e24048, 2024, https://doi.org/10.1016/j.heliyon.2024.e24048

## Nomenclature

| | | | |
|---|---|---|---|
| c | Length of chord-line [m] | R | Turbine radius [m] |
| $C_p$ | Pressure Coefficient | V | Velocity [m/s] |
| D | Turbine Diameter [m] | $u_{i,j}$ | Velocity component [m/s] |
| $e_a$ | Error estimation | $Y^+$ | Non dimensional wall distance |
| $f_i$ | Dependent Variable (i=1, 2, 3) | $\lambda$ | Solidity of the turbine |
| $g_i$ | Gravitational accelaration | $\omega$ | Rotational Velocity (rad/s) |
| H | Height of Turbine [m] | $\tau_{ij}$ | Stress Tensor |
| $h_i$ | Grid size (i=1, 2, 3) | $\bar{G}_\omega$ | Production of Turbulent Kinetic |
| $k$ | Kinetic Energy | $Y_k$ | Energy [$m^2/s^3$] |
| N | Number of blades | $S_k$ | Dissipation [$m^2/s^3$] |
| P | Pressure (Pa) | | Source [$m^2/s^3$] |